Compressive behaviour of circular steel tube-confined concrete stub columns with active and passive confinement

Mahdi Nematzadeh [1], Iman Hajirasouliha [*2], Akbar Haghinejad [1] and Morteza Naghipour [3]

[1] *Department of Civil Engineering, University of Mazandaran, Babolsar, Iran*
[2] *Department of Civil and Structural Engineering, University of Sheffield, Sheffield, UK*
[3] *Faculty of Civil Engineering, Babol Noshirvani University of Technology, Babol, Iran*

Abstract. This paper presents the results of a comprehensive experimental investigation on the compressive behaviour of steel tube-confined concrete (STCC) stub columns with active and passive confinement. To create active confinement in STCC columns, an innovative technique is used in which steel tube is laterally pre-tensioned while the concrete core is simultaneously pre-compressed by applying pressure on fresh concrete. A total of 135 STCC specimens with active and passive confinement are tested under axial compression load and their compressive strength, ultimate strain capacity, axial and lateral stress–strain curves and failure mode are evaluated. The test variables include concrete compressive strength, outer diameter to wall thickness ratio of steel tube and prestressing level. It is shown that applying active confinement on STCC specimens can considerably improve their mechanical properties. However, applying higher prestressing levels and keeping the applied pressure for a long time do not considerably affect the mechanical properties of actively confined specimens. Based on the results of this study, new empirical equations are proposed to estimate the axial strength and ultimate strain capacity of STCC stub columns with active and passive confinement.

Keywords: compressive behaviour; pre-compressed concrete; active confinement; steel tube-confined concrete; stub column

1. Introduction

Applications of steel tube confined concrete (STCC) columns have been extensively increased in modern construction due to their good structural performance and high ductility. In STCC columns the load is only applied on the concrete core, which can effectively delay the local buckling of steel tubes. This can increase the load bearing capacity of the composite section compared to the case that the load is applied simultaneously on the concrete core and the steel tube (O'Shea and Bridge 1998, Fam *et al*. 2004). In addition, using STCC columns eliminates the need for concrete formwork and curing during the construction process and, therefore, reduce the construction time and cost.

Extensive research has been conducted to study the axial load capacity of STCC columns (e.g., Xiao *et al*. 2005, Han *et al*. 2005, Qi *et al*. 2011, Fu *et al*. 2011, Huang *et al*. 2012, Dong *et al*. 2015). In general, the results of these studies indicated high levels of ductility in STCC columns. Han *et al*. (2008) performed a parametric study on STCC stub columns subjected to axial local compression loads. They showed that the confining pressure of the concrete core and the ultimate strength capacity of STCC columns are reduced

by increasing the outer diameter-to-wall thickness ratio of steel tubes. In a follow-up study, Yu *et al*. (2010) developed a finite element model, validated based on the experimental results of Han *et al*. (2005), to study the compressive behaviour of STCC columns. It was found that, in general, STCC columns exhibit high levels of ductility and energy dissipation capacity, particularly when they are subjected to high axial loads.

Applying an external active confinement can improve the compressive behaviour and deformation capacity of reinforced concrete (RC) columns by delaying the offset of initial cracks in the concrete core. Mortazavi *et al*. (2003) developed a new strengthening technique for existing concrete columns by using additive expansive materials in the concrete mix to apply lateral pre-tensioning loads. The results of their study showed that RC columns confined with pre-tensioned FRP (Fibre Reinforced Polymer) material exhibit up to 35% higher load-carrying capacity compared to the similar columns without pre-tensioning. By using a similar prestressing technique, Chang *et al*. (2009) investigated experimentally and analytically the mechanical characteristics of prestressed concrete-filled steel tube columns (PCFT) under eccentric loading. They concluded that eccentrically loaded PCFT columns generally have higher load carrying capacities compared to similar conventional concrete filled steel tubes. The experimental and analytical study conducted by Shinohara (2008) also showed the effectiveness of active confinement to improve the shear load capacity of high-strength concrete columns

---

*Corresponding author,
Associate Professor, Senior Lecturer,
E-mail: i.hajirasouliha@sheffield.ac.uk

by using transverse prestressing. Janke *et al*. (2009) conducted an experimental study on the load-bearing capacity of prestressed confined concrete columns, which confirmed the beneficial effects of confinement prestressing on the residual load bearing capacity.

Krstulovic-Opara and Thiedeman (2000) investigated the use of self-stressing composites for the active confinement of concrete members. By using a similar prestressing method, Andrawes *et al*. (2010) and Shin and Andrawes (2014) used shape memory alloys (SMAs) spirals to provide active confinement in RC columns. It was shown that even under a small confining pressure the concrete strength and ductility is considerably improved. Moghaddam *et al*. (2010) studied the axial compressive behaviour of concrete specimens with active confinement using high-strength Post-Tensioned Metal Straps (PTMS). The results of their experimental study on 72 cylindrical and prismatic compressive specimens showed that PTMS can considerably increase the compressive strength and ductility of the concrete specimens, while the gain in strength is dependent on the effective mechanical volumetric ratio of confining strips. In a follow-up study, Helal *et al*. (2016) investigated the effectiveness of using PTMS at enhancing the bond behaviour of short lap spliced steel bars in RC beams. Vincent and Ozbakkaloglu (2015) conducted an experimental investigation on the influence of prestressing Aramid FRP (AFRP) confining shells on the axial compressive behaviour of high-strength concrete-filled FRP tube columns. The results of their study indicated that prestressing can prevent the sudden drop in strength typically observed in FRP-confined high-strength concrete specimens.

This paper presents an innovative technique to apply active confinement in STCC stub columns, in which the steel tube is pre-tensioned in the circumferential direction by applying pressure on the fresh concrete. The proposed method does not need vibration, while it can provide high prestressing levels and therefore improve the load bearing capacity of composite columns without using any additional material. This technique was introduced by Nemati (2006) and then further developed by Nematzadeh (2012) and Nematzadeh *et al*. (2017). In this study, extensive experimental tests are conducted to investigate the mechanical properties of STCC stub columns with active and passive

confinement, including their axial and lateral stress–strain behaviour, compressive strength and failure mode. The test variables are concrete compressive strength, outer diameter to wall thickness ratio of the steel tube and prestressing level. Based on the results of this study, empirical equations are proposed to estimate the failure compressive strength and ultimate strain of actively and passively confined specimens.

2. Experimental program

2.1 Materials

The concrete mix design was based on ACI 211 (2008) recommendations using crushed stone (maximum size of 12.5 mm), fluvial sand and Type I Portland cement. No additive material was used in the concrete mix. To investigate the effect of concrete compressive strength, a range of nominal concrete strengths were obtained including 15, 25, 35, 45, 47, 50 and 55 MPa.

The steel tubes of STCC specimens were seamless and hot-rolled with 55.5 mm inner diameter, 150 mm height and outer diameter to wall thickness ratios of 24.2, 29.8, 39 and 57.5. The mechanical properties of the steel tubes are presented in Table 1, in which ε_y, ε_p and ε_u are strains at the yielding, strain hardening and ultimate points, respectively; f_y and f_{us} are yield strength and ultimate strength of steel tube; v_s is Poisson's ratio; and E_s and E'_s are the initial modulus of elasticity and strain hardening modulus of elasticity of steel tube. Fig. 1 shows the test device used for determining the mechanical properties of steel tubes per ASTM A370 (2003).

2.2 Test specimens

In this study, 15 groups of confined concrete specimens with different values of concrete strength, outer diameter to wall thickness ratio and prestressing level were tested under

Table 1 Mechanical properties of steel tube

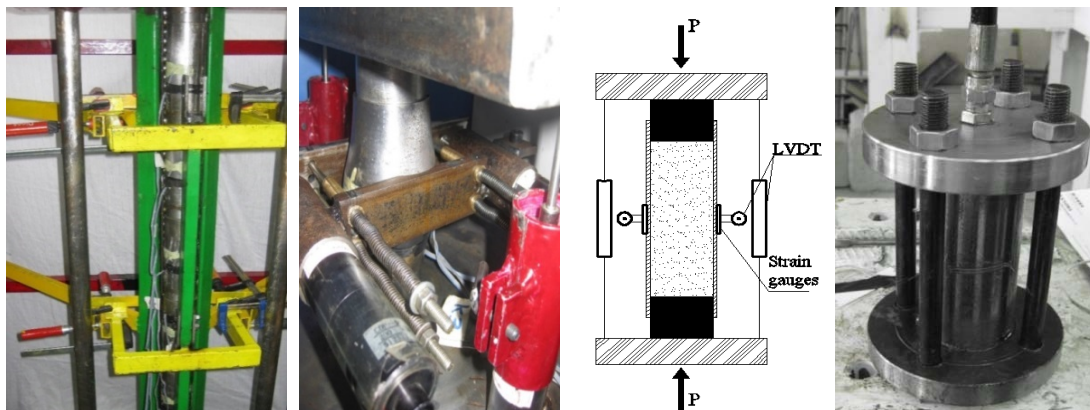| f_y (MPa)	f_{us} (MPa)	E_s (GPa)	E'_s/E_s	v_s	$\varepsilon_p/\varepsilon_y$	$\varepsilon_u/\varepsilon_y$
339	480	210	0.0226	0.28	8.6	70.9

Fig. 1 Test setup for actively confined specimens

Table 2 Specifications of tested specimens

Specimen ID	D/t	Nominal compressive strength of reference concrete (MPa)	Initial hoop strain of steel tube in μs (Initial lateral pressure P_i in MPa)	Final hoop strain of steel tube in μs (Final lateral pressure P_f in MPa)	Total pressure loss (%)
L25P350-2.5	24.2	25	367.2 (6.9)	233.3 (4.4)	36.5
S25P350-2.5	24.2	25	367.2 (6.9)	98.4 (1.9)	73.2
N25P350-2.5	24.2	25	-	-	-
L25P950-1.5	39.0	25	1006.6 (11.4)	729.4 (8.3)	27.5
S25P950-1.5	39.0	25	1006.6 (11.4)	179.0 (2.0)	82.2
N25P950-1.5	39.0	25	-	-	-
L25P650-1.5	39.0	25	628.0 (7.1)	399.7 (4.5)	36.4
S25P650-1.5	39.0	25	628.0 (7.1)	100.7 (1.1)	84.0
N25P650-1.5	39.0	25	-	-	-
L35P650-1.5	39.0	35	658.0 (7.5)	400.5 (4.5)	39.1
S35P650-1.5	39.0	35	658.0 (7.5)	119.5 (1.4)	81.8
N35P650-1.5	39.0	35	-	-	-
L15P650-1.5	39.0	15	658.0 (7.5)	400.5 (4.5)	39.1
S15P650-1.5	39.0	15	658.0 (7.5)	119.5 (1.4)	81.8
N15P650-1.5	39.0	15	-	-	-
L25P950-2.5	24.2	25	964.0 (18.2)	596.0 (11.3)	38.2
S25P950-2.5	24.2	25	964.0 (18.2)	168.7 (3.2)	82.5
N25P950-2.5	24.2	25	-	-	-
L50P650-2.5	24.2	50	629.7 (11.9)	321.8 (6.1)	48.9
S50P650-2.5	24.2	50	629.7 (11.9)	115.3 (2.2)	81.7
N50P650-2.5	24.2	50	-	-	-
L15P550-2.5	24.2	15	543.5 (10.3)	267.8 (5.1)	50.7
S15P550-2.5	24.2	15	543.5 (10.3)	109.3 (2.1)	79.9
N15P550-2.5	24.2	15	-	-	-
L35P550-2.5	24.2	35	543.5 (10.3)	267.8 (5.1)	50.7
S35P550-2.5	24.2	35	543.5 (10.3)	109.3 (2.1)	79.9
N35P550-2.5	24.2	35	-	-	-
L25P500-2.5	24.2	25	483.9 (9.2)	268.9 (5.1)	44.4
S25P500-2.5	24.2	25	483.9 (9.2)	64.5 (1.2)	86.7
N25P500-2.5	24.2	25	-	-	-
L25P650-2.0	29.8	25	604.9 (9.2)	336.2 (5.1)	44.4
S25P650-2.0	29.8	25	604.9 (9.2)	80.6 (1.2)	86.7
N25P650-2.0	29.8	25	-	-	-
L45P650-1.5	39.0	45	597.0 (6.8)	343.0 (3.9)	42.5
S45P650-1.5	39.0	45	597.0 (6.8)	203.3 (2.3)	65.9
N45P650-1.5	39.0	45	-	-	-
L25P2000-1.0	57.5	25	1614.3 (12.2)	1159.0 (8.8)	28.2
S25P2000-1.0	57.5	25	1614.3 (12.2)	420.3 (3.2)	74.0
N25P2000-1.0	57.5	25	-	-	
L47P650-1.5	39.0	47	607.6 (6.9)	315.2 (3.6)	48.1
S47P650-1.5	39.0	47	607.6 (6.9)	90.5 (1.0)	85.1
N47P650-1.5	39.0	47	-	-	-
L55P650-2.5	24.2	55	689.2 (13.0)	346.0 (6.5)	49.8
S55P650-2.5	24.2	55	689.2 (13.0)	51.0 (1.0)	92.6
N55P650-2.5	24.2	55	-	-	-
Average for LPSTC specimens (COV%)					41.6 (18.2)
Average for SPSTC specimens (COV%)					81.2 (7.9)

axial compression loads. Each group consisted of three series including long-term prestressed steel tube-confined compressed concrete (LPSTC), short-term prestressed steel tube-confined compressed concrete (SPSTC) and non-prestressed steel tube-confined concrete (NPSTC) specimens. The difference between the two groups of actively confined specimens, LPSTC and SPSTC, is the duration of the applied pressure, which is 6 days and 15–30 min, respectively.

Table 2 shows the specification of the tested specimens. It should be noted that to ensure repeatability of the tests, three replicate samples were prepared for each case (135 confined concrete specimens in total) and the mean values of the results were considered. Also, for each test group three uncompressed concrete specimens were prepared as reference samples. The first letter of each specimen ID shows the type of confined concrete (L, S and N represent LPSTC, SPSTC and NPSTC specimens, respectively), the first number indicates the nominal compressive strength of the reference concrete in MPa, the second number (after the letter P) gives the design prestressing level in terms of steel tube hoop strain in microstrain, and the last number shows the thickness of the steel tube in mm. For example, S25P350-2.5 represents the SPSTC Specimen with the nominal reference concrete compressive strength of 25 MPa, design steel tube hoop strain of 350 microstrain and steel tube thickness of 2.5 mm.

2.3 Instrumentation and test set up

To create active confinement in STCC specimens, a novel fabricated prestressing device is used as shown in Fig. 1. By placing STCC specimens into the device and applying pressure on fresh concrete, the concrete core is compressed and the steel tube is pretensioned in hoop directions. To determine the initial lateral pressure and the final lateral pressure (known as the prestressing level) applied on the confined concrete, the hoop strains are measured on the steel tube by using strain gauges installed on the outer surface of the tube at the mid-height.

To conduct compression tests on confined and unconfined concrete specimens, a 2000 kN capacity ELE testing machine was used as shown in Fig. 1. The specimens were subjected to monotonic axial loading at an average load rate of 42 kN/min until failure. At the two ends of the confined specimens, solid steel cylinders (with a height of 50 mm and a diameter of 55.4 mm) were used to apply compressive loads only on the concrete core. The axial deformation of the concrete core in the confined specimens was determined by using two longitudinal linear variable differential transducers (LVDTs) installed symmetrically on both sides of the STCC specimens and between the loading platens. Also, two horizontal LVDTs were placed symmetrically at the mid-height of the specimens to measure the lateral deformations. Moreover, to record the strain and stress levels of the steel tubes during the loading process, longitudinal and hoop strain gauges were installed on the outer wall of the steel tubes at the mid-height. Finally, tensile tests were carried out on the steel tubes to calculate their mechanical properties such as yield strength, ultimate strength, modulus of elasticity and

Poisson's ratio as recommended by ASTM A370. For each test specimen, the initial and final hoop strains of the steel tube are presented in Table 2. Further details of the prestressing device are described in Nematzadeh and Naghipour (2012).

3. Test results and discussion

3.1 Prestressing force

To investigate the effects of prestressing force on the characteristics of STCC columns, different levels of initial lateral pressure were applied within the range of 6.8-18.2 MPa. Fig. 2 illustrates the hoop strains versus time for two typical actively confined specimens; L15P650-1.5 and S15P650-1.5 with long-term and short-term prestressed steel tube-confined compressed concrete, respectively. It can be seen that in the LPSTC specimen (L15P650-1.5) a significant pressure loss occurred at the first day, mainly because of the gradual extraction of the concrete water owing to the continuously applied pressure. A considerable pressure loss took place after removing the prestressing device on day 6. This was attributed to the changes in the stress condition of confined concrete from triaxial compression into biaxial compression. Subsequently, the applied pressure was slightly reduced, which seems to be due to the concrete shrinkage. As shown in Fig. 2, a sudden loss occurred in the SPSTC specimen (S15P650-1.5) immediately after applying the initial pressure, which was caused by removing the specimen from the prestressing device. It should be noted that the friction between the aggregates does not allow the hoop strain of steel tube to vanish. It can also be seen from the figure that the pressure loss is the SPSTC specimen was negligible after the first day.

Based on the results presented in Table 2, the average total pressure loss for LPSTC specimens was 41.6% with a coefficient of variation (COV) of 18.2%, while for SPSTC specimens the average loss was 81.2% with a COV of 7.9%. This implies that the pressure loss is considerably higher in the cases of using short-term prestressed steel tubes (i.e., SPSTC specimens). Based on experimental results of this study, the following equations are proposed to
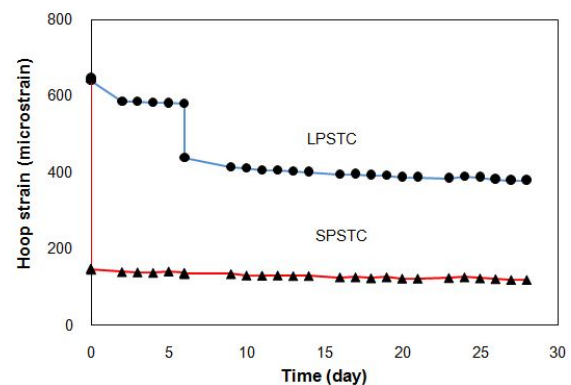
Fig. 2 Steel tube hoop strain–time curve for actively confined specimens

predict the final prestressing level for SPSTC and LPSTC specimens

$$P_f = 0.19 P_i \qquad \text{for SPSTC} \qquad (1)$$

$$P_f = 0.58 P_i \qquad \text{for LPSTC} \qquad (2)$$

where P_i and P_f are the initial and final pressure (prestressing level), respectively.

3.2 Failure compressive strength

In this section, the compressive strength of actively and passively confined specimens at the failure point is evaluated. The compressive strength of confined concrete is a function of the compressive strength of the corresponding unconfined concrete and the level of confining pressure on the concrete core. In one of the early attempts, Richart *et al.* (1928) suggested a linear equation to evaluate the compressive strength of confined concrete material

$$f_{cc} = f_c(1 + 4.1 \frac{f_l}{f_c}) \qquad (3)$$

where f_{cc} and f_c are the compressive strength of confined and unconfined concrete, respectively, and f_l is the confining pressure. The confinement ratio is defined as the ratio of confining pressure to the compressive strength of unconfined concrete (f_l / f_c) and is denoted by C_r in this study.

It should be noted that Eq. (3) suggests a linear relationship between the relative increase in the confined compressive strength and the confinement ratio. To improve the efficiency of this equation, Mander *et al.* (1988) proposed the following non-linear relationship to predict the concrete compressive strength under different confinement levels

$$f_{cc} = f_c(-1.254 + 2.254 \sqrt{1 + \frac{7.94 f_l}{f_c}} - 2\frac{f_l}{f_c}) \qquad (4)$$

The accuracy of Eqs. (3) and (4) will be investigated in the following section against the experimental tests on NPSTC specimens in this study.

3.2.1 NPSTC specimens

The experimental results in this study showed that NPSTC specimens reach their ultimate strength at the failure point. This is because the concrete core of the NPSTC specimens has high confinement ratio and, therefore, no softening (descending branch) is observed in their stress–strain curve. As shown in Table 3, the failure compressive strength of the NPSTC specimens was between 83.7 and 261.1 MPa with a COV in the range of 0.8%-6.1%. It can be noted that, depending on the wall thickness, the relative increase in the compressive strength of NPSTC specimens was 3 to 13 times higher than the corresponding unconfined concrete specimens.

Fig. 3 illustrates the increase in the failure strength versus the steel tube wall thickness for four specimens having almost similar unconfined concrete compressive strength. It can be noticed from the figure that by increasing the wall thickness, the relative increase in the failure strength increases almost linearly.

Due to the friction at the interface of the concrete core and steel tube in STCC specimens and the resulting interface shear stress, a longitudinal compressive stress is always developed in the steel tube, which leads to a reduction in the confining pressure. In this study, the von

Table 3 Compressive strength of NPSTC specimens at the failure point

Specimen ID	Experimental failure compressive strength in MPa (f_{cc})	Compressive strength of unconfined concrete in MPa (f_c)	Failure confined compressive strength in MPa (f_{pf})	Predicted failure compressive strength in MPa (P_{pf}/A_c)
N25P350-2.5	219.1 (2.2)	28.2	185.0	216.1
N25P950-1.5	123.8 (1.1)	31.7	103.7	144.1
N25P650-1.5	138.3 (3.9)	28.3	118.2	140.7
N35P650-1.5	122.6 (4.9)	42.4	102.5	154.8
N15P650-1.5	123.1 (4.2)	20.5	103.0	132.9
N25P950-2.5	227.7 (5.4)	30.0	193.6	217.9
N50P650-2.5	221.2 (5.0)	50.5	187.1	238.4
N15P550-2.5	212.8 (6.1)	16.7	178.7	204.6
N35P550-2.5	229.0 (1.8)	37.1	194.9	225.0
N25P500-2.5	224.8 (5.4)	27.2	190.7	215.1
N25P650-2.0	175.6 (2.7)	27.2	148.5	177.3
N45P650-1.5	138.6 (2.3)	45.4	118.5	157.8
N25P2000-1.0	83.7 (2.4)	25.9	70.4	100.7
N47P650-1.5	141.5 (2.2)	46.9	121.4	159.3
N55P650-2.5	261.1 (0.8)	52.6	227.0	240.5

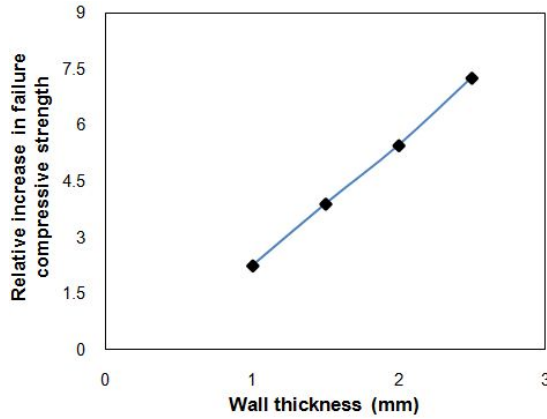*Note: The numbers in parentheses shows COV in %

Fig. 3 Relative increase in the failure compressive strength of NPSTC specimens compared to the corresponding unconfined concrete as a function of steel tube wall thickness

Mises yield criterion (Hosford 2010) was used to estimate the steel yield point. Fig. 4(a) illustrates the longitudinal stress versus the hoop stress of the steel tube for a typical NPSTC specimen (N45P650-1.5) in the elastic stage (before yielding). It is shown that the longitudinal compressive stress of the steel tube was almost twice the hoop tensile stress at the yielding point. Before reaching the yield point, a discontinuity is observed in the longitudinal stress–hoop stress curve of NPSTC specimens, which is due to the relative slippage between the concrete core and the steel tube. This leads to a faster increase in the hoop stress compared to the longitudinal stress.

After the initiation of yielding, the longitudinal compressive stress is reduced while the hoop tensile stress increases due to the considerable dilation of the concrete core. This trend can be observed in Fig. 4(b), in which the curve is the von-Mises yield surface. According to the results, on average, the ratio of the longitudinal stress to the hoop stress of the steel tube is close to 1 at the end of the yield curve.

In the strain hardening stage and up to the failure point, the hoop tensile stress of steel tube is increased while the longitudinal compressive stress is almost constant. It is

shown that the longitudinal to hoop stress ratio of the steel tube at the failure point is about 0.5.

According to the von Mises criterion and by considering $\dfrac{\sigma_z}{\sigma_\theta} = \alpha$, the hoop stress of the steel tube at the failure point can be obtained as a function of α and f_{us} (ultimate strength of steel tube) as follows

$$\sigma_\theta = \frac{f_{us}}{\sqrt{1 + \alpha + \alpha^2}} \tag{5}$$

where σ_z and σ_θ are the longitudinal compressive stress and the hoop tensile stress of the steel tube, respectively. By using Eq. (5) and the classical theory of thin-walled tubes as $f_{lu} = 2t\sigma_\theta / (D - 2t)$, the confining pressure at the failure point (f_{lu}) can be calculated as follows
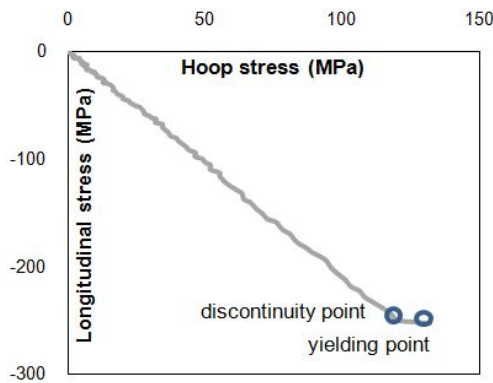
$$f_{lu} = \frac{2tf_{us}}{(D - 2t)\sqrt{1 + \alpha + \alpha^2}} \tag{6}$$

where D and t are outer diameter and wall thickness of steel tubes, respectively. The failure confining pressure of NPSTC specimens obtained from Eq. (6) is between 13.1 and 32.7 MPa, while the failure confinement ratio ($C_{ru} = f_{lu}/f_c$) is between 0.42 and 1.96. The axial load-carrying capacity of the concrete core in NPSTC specimens can be easily calculated from the difference between the load-carrying capacity of the composite section and that of the steel tube. The ultimate strength of NPSTC specimens corresponding to the axial load-carrying capacity of the concrete core is known as failure confined compressive strength (f_{pf}), the values of which are given in Table 3.
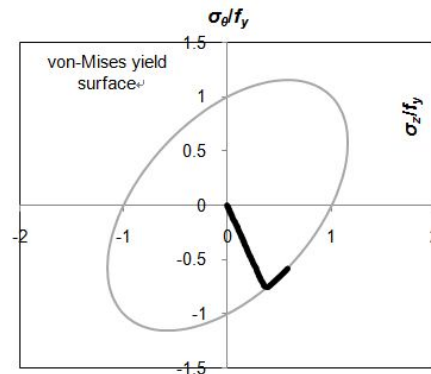
Based on the results of this study, the following linear relationship is proposed between the relative increase in the confined compressive strength and the confinement ratio of NPSTC specimens at the failure point

$$\frac{(f_{pf} - f_c)}{f_c} = 4.70 C_{ru} \tag{7}$$

The ratio of the relative increase in the confined compressive strength to the confinement ratio is known as

(a) Steel tube longitudinal stress–hoop stress curve in the elastic stage

(b) Normalized longitudinal stress–hoop stress curve in the elastic and yield stages

Fig. 4 longitudinal stress versus the hoop stress in a typical NPSTC specimen (N45P650-1.5)
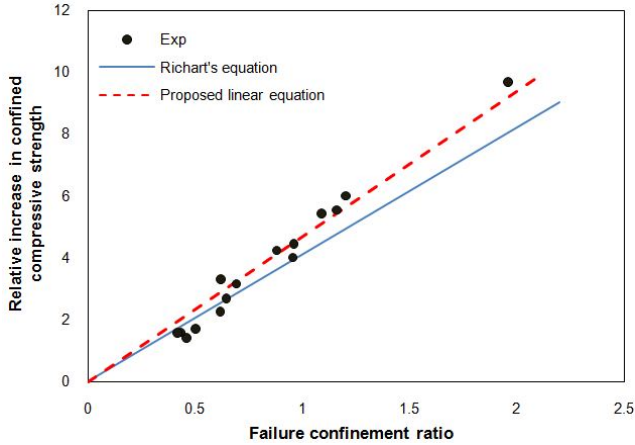
Fig. 5 Relative increase in confined compressive strength of NPSTC specimens versus failure confinement ratio based on the proposed linear equation and Richart's equation

the "confinement effectiveness coefficient" denoted as k. The confinement effectiveness coefficient calculated from the above equation is equal to 4.7, which is about 15% higher than the corresponding value in Richart's equation (see Eq. (3)). It is shown in Fig. 5 that the proposed empirical linear equation has a better agreement with the experimental results of NPSTC specimens (Coefficient of determination R^2 = 0.96) compared to the Richart's equation.

Based on the results of this study, the following non-linear equation is also suggested to calculate the failure confined compressive strength of NPSTC specimens, which is more accurate compared to the proposed linear equation (Eq. (7))

$$\frac{(f_{pf} - f_c)}{f_c} = \frac{16.4 C_{ru}^2}{1 + 2.07 C_{ru} + 0.37 C_{ru}^2} \qquad (8)$$

The relationship obtained from Eq. (8) along with the experimental data is illustrated in Fig. 6. It can be seen that
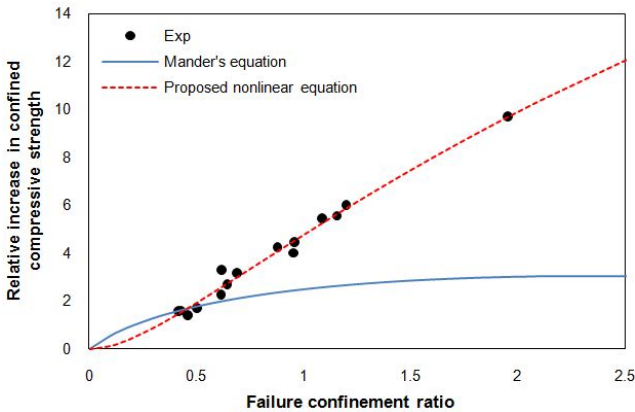

Fig. 6 Relative increase in confined compressive strength of NPSTC specimens versus failure confinement ratio based on the proposed nonlinear equation and Mander's equation

the regression curve is in a very good agreement with the experimental results (R^2 = 0.98). It is shown in Fig. 6 that there is an upward concavity (positive concavity) for confinement ratios lower than 0.5, so that by increasing the confinement ratio the gradient of the curve increases rapidly. For confinement ratios ranging from 0.5 to 1.7, the relationship between the relative increase in confined compressive strength and failure confinement ratio is almost linear. For confinement ratios higher than 1.7, the gradient of the curve decreases significantly with increasing the confinement ratio. This indicates that the effectiveness of the confinement is considerably reduced in very high confinement ratios, which is in agreement with the results obtained by other researchers such as Mander *et al.* (1988). However, it is shown in Fig. 6 that, unlike the proposed nonlinear equation, Mander's equation does not provide acceptable results for the NPSTC specimens with the failure confinement ratios above 0.5.

The load-carrying capacity of NPSTC specimens at the failure point (P_{pf}) can be determined by adding the confined compressive strength to the axial strength of the steel tube as follows

$$P_{pf} = A_s f_{us} \frac{\alpha}{\sqrt{1 + \alpha + \alpha^2}} + A_c (f_c + k \frac{2 t f_{us}}{(D - 2t)\sqrt{1 + \alpha + \alpha^2}}) \quad (9)$$

where A_s and A_c are the cross section of steel tube and concrete core, respectively. By replacing k = 4.7 and α = 0.5 in Eq. (9), the above equation can be rewritten as

$$P_{pf} = 0.38 A_s f_{us} + (1 + 7.11 \frac{t f_{us}}{(D - 2t) f_c}) A_c f_c \qquad (10)$$

The compressive strength values obtained from Eq. (10) are presented in Table 3 for all NPSTC specimens. According to this table, the ratio of the experimental to predicted failure compressive strength is on average 1.06 (between 0.92 and 1.26), which indicates the good accuracy of the proposed equation.

3.2.2 PSTC specimens

The compressive strengths of SPSTC and LPSTC specimens at their failure point are given in Table 4. It is shown that the failure strength of LPSTC specimens is between 93.6 and 265.7 MPa with COV ranging from 1.4% to 6.5%. Similarly, the failure strength of SPSTC specimens is between 94.1 and 253.3 MPa with COV ranging from 0.3% to 8.9%. There is a small difference between the failure strength of SPSTC and LPSTC specimens, which shows that increasing the prestressing level has a negligible effect on the failure strength of PSTC specimens. This also implies that applying a long-term pressure and higher prestressing levels to improve the failure strength of PSTC specimens is not very efficient. Fig. 7 shows the failure compressive strength versus steel tube wall thickness of four SPSTC and LPSTC specimens with almost identical concrete compressive strength. It can be seen that the results of SPSTC and LPSTC specimens are almost similar, which is in agreement with the previous observations.

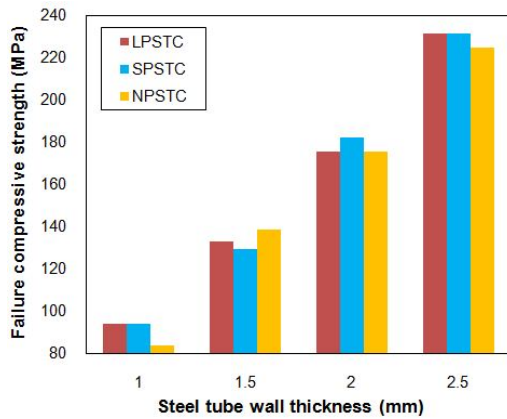In is shown in Table 4 that the ratios of the failure

Fig. 7 Failure compressive strength versus steel tube wall thickness for actively and passively confined specimens

strength of PSTC to the corresponding NPSTC specimens are between 0.92 and 1.13 (with an average of 1.02). These results indicate that prestressing the confinement using the present technique has a negligible effect on the failure strength of STCC specimens. Fig. 7 shows the good agreement between the failure strength of NPSTC and PSTC specimens for different steel tube wall thicknesses. The reason is that prestressing the PSTC specimens leads to earlier failure of the steel tube compared to the NPSTC specimens and, therefore, the possibility of improving the compressive strength of the confined specimens at the failure point is considerably reduced.

Unlike NPSTC specimens in which the failure compressive strength is considered as the ultimate strength, in PSTC specimens the compressive strength at the failure point is sometimes lower than the compressive strength at the initial peak point (this can be seen later in stress-strain curves).

Table 4 Results of compressive strength of PSTC specimens at the failure point

Specimen ID	Experimental failure compressive strength in MPa (f_{cc})	Compressive strength of unconfined compressed concrete in MPa (f_{co})	Failure confined compressive strength in MPa (f_{af})	Predicted failure compressive strength in MPa (= P_{af} / A_c)
L25P350-2.5	230.3 (4.8)	63.5	211.3	233.8
S25P350-2.5	224.7 (2.6)	61.3	205.7	234.0
L25P950-1.5	130.5 (5.8)	67.7	119.3	132.4
S25P950-1.5	130.4 (3.3)	64.8	119.2	132.3
L25P650-1.5	133.0 (3.8)	63.6	121.8	132.3
S25P650-1.5	129.2 (5.8)	61.4	118.0	132.5
L35P650-1.5	130.8 (2.6)	75.5	119.6	133.6
S35P650-1.5	138.5 (0.3)	69.9	127.3	132.6
L15P650-1.5	127.3 (2.6)	51.4	116.1	135.0
S15P650-1.5	125.4 (5.2)	50.4	114.2	135.4
L25P950-2.5	232.6 (6.5)	65.7	213.6	233.4
S25P950-2.5	239.2 (2.4)	63.2	220.2	233.9
L50P650-2.5	234.2 (1.8)	76.4	215.2	229.2
S50P650-2.5	240.1 (7.0)	68.1	221.1	232.6
L15P550-2.5	212.4 (4.6)	44.0	193.4	217.4
S15P550-2.5	221.6 (3.5)	43.5	202.6	216.2
L35P550-2.5	216.8 (2.2)	72.6	197.8	230.9
S35P550-2.5	226.2 (5.6)	68.4	207.2	232.5
L25P500-2.5	231.5 (3.4)	62.1	212.5	234.0
S25P500-2.5	231.2 (3.2)	60.1	212.2	234.0
L25P650-2.0	175.3 (4.6)	62.1	160.2	182.8
S25P650-2.0	182.3 (8.9)	60.1	167.2	183.7
L45P650-1.5	139.2 (1.4)	76.4	128.0	133.8
S45P650-1.5	134.0 (3.6)	69.8	122.8	132.6
L25P2000-1.0	93.6 (5.4)	60.2	86.2	92.7
S25P2000-1.0	94.1 (1.6)	58.4	86.7	91.8
L47P650-1.5	135.7 (4.0)	76.6	124.5	133.9
S47P650-1.5	130.5 (5.9)	69.5	119.3	132.5
L55P650-2.5	265.7 (6.4)	76.0	246.7	229.4
S55P650-2.5	253.3 (2.9)	66.9	234.3	233.0

*Note: The numbers in parentheses shows COV in %

This trend is usually observed in the specimens with the failure confinement ratio lower than 0.35. It should be noted that in PSTC specimens, the initial peak point is defined as the first relative maximum in axial stress–strain curve, which occurs in the vicinity of the strain hardening point of the steel tube. The initial peak strength is considered as the ultimate strength of the specimens with a low confinement ratio. In these specimens, using strong concrete core and weak steel tube can change the behaviour of the composite section to the concrete behaviour, in which the maximum strength occurs at low deformation levels.

To investigate the effect of confinement level (through prestressing the steel tube) on the failure strength of PSTC specimens, the relative increase in their failure strength compared to the corresponding unconfined concrete is calculated from Table 4. It should be noted that the concrete core of PSTC specimens is compressed and, therefore, its properties is improved relative to the reference concrete specimens. Therefore, to evaluate the effect of active confinement on the performance of the confined concrete, the relative increase in the compressive strength of PSTC specimens is compared to that of the unconfined compressed concrete. According to the experimental results, the relative increase in the failure strength for LPSTC specimens is between 55% and 383%, while for SPSTC specimens is between 61% and 409%.

By using the Mises yield criterion and the isotropic hardening model for PSTC specimens, the longitudinal to hoop stress ratio of the steel tube is calculated equal to 0.5 and 0.24 at the strain hardening and failure points, respectively. Using Eqs. (5) and (6) and by replacing $\alpha = 0.24$, the hoop stress and confining pressure of PSTC specimens at the failure point can be calculated as follows

$$\sigma_\theta = 0.878 f_{us} \tag{11}$$

$$f_{lu} = \frac{1.756 t f_{us}}{(D - 2t)} \tag{12}$$

The confinement ratio of PSTC specimens at the failure point can be obtained from the ratio of the confining pressure (Eq. (12)) to the compressive strength of unconfined compressed concrete (f_{co}) as follows

$$C_{ru} = \frac{1.756 t f_{us}}{(D - 2t) f_{co}} \tag{13}$$

The values of f_{co} for all PSTC specimens are given in Table 4. Based on the Eqs. (12) and (13), the confining pressure of PSTC specimens at the failure point is between 15.2 and 38.0 MPa, while the confinement ratio is calculated to be between 0.25 and 0.87.

The prestressing ratio (P_r) is defined as the ratio of prestressing level (final pressure) to the compressive strength of unconfined compressed concrete, as follows

$$P_r = \frac{P_f}{f_{co}} \tag{14}$$

In this study, the prestressing ratio for SPSTC and

LPSTC specimens was within the range of 0.014-0.055 and 0.047-0.172, respectively. This indicates that the prestressing ratio of LPSTC specimens can be up to 3 times higher than that of SPSTC specimens.

The confined compressive strength of PSTC specimens can be obtained by subtracting the steel tube longitudinal strength from the compressive strength of the composite section. The confined compressive strengths of PSTC specimens at their failure point are provided in Table 4. It is shown that the confined compressive strength of SPSTC specimens is between 86.7 and 234.3 MPa, while for LPSTC specimens is between 86.2 and 246.7 MPa. In addition, the relative increase in the failure confined compressive strength compared to the unconfined compressed concrete strength is in the range of 48%–366% and 43%-340% for SPSTC and LPSTC specimens, respectively. Based on the nonlinear regression analysis of the experimental results, the following relationship is proposed between the relative increase in the confined compressive strength and the confinement ratio at the failure point

$$\frac{f_{af} - f_{co}}{f_{co}} = \frac{4.657 C_{ru}^2}{1 - 1.61 C_{ru} + 1.85 C_{ru}^2} \tag{15}$$

where f_{af} is the failure confined compressive strength of PSTC specimens. The left side of the equation represents the relative increase in the failure confined strength of PSTC specimens compared to the unconfined compressed concrete strength. The above equation can be applied to both SPSTC and LPSTC specimens. Fig. 8 compares the relative increase in the failure confined strength calculated from Eq. (15) with the experimental results of PSTC specimens. As can be seen, there is a very good agreement between the empirical and experimental results ($R^2 = 0.98$). Based on Eq. (15), the confinement effectiveness coefficient in the actively confined specimens was between 1.7 and 4.1, which is about 0.4 to 0.9 times the corresponding values in the passively confined specimens.

The load-carrying capacity of PSTC specimens (P_{af}) at their failure point can be calculated by adding the confined
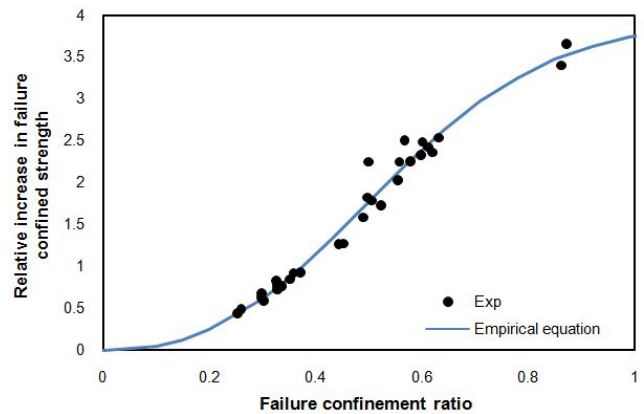

Fig. 8 Relative increase in the failure confined compressive strength of PSTC specimens compared to the unconfined compressed concrete strength as a function of failure confinement ratio

compressive strength of concrete core to the longitudinal strength of steel tube as shown in Eq. (16). This equation is similar to the Eq. (9) that is obtained for NPSTC specimens except that f_{co} is replaced by f_c

$$P_{af} = A_s f_{us} \frac{\alpha}{\sqrt{1+\alpha+\alpha^2}} + A_c \left[f_{co} + k \frac{2t f_{us}}{(D-2t)\sqrt{1+\alpha+\alpha^2}} \right] \quad (16)$$

The confinement effectiveness coefficient (k) can be then determined by replacing Eq. (15) in the following equation

$$k = \frac{(f_{af} - f_{co})/f_{co}}{C_{ru}} \quad (17)$$

By replacing k and $\alpha = 0.24$ in Eq. (16), the failure load-carrying capacity of PSTC specimens can be obtained as follows

$$P_{af} =$$
$$0.21 A_s f_{us} + A_c f_{co} \left[1 + \frac{8.18 C_{ru} t f_{us}}{(D-2t)(1-1.61 C_{ru} + 1.85 C_{ru}^2) f_{co}} \right] \quad (18)$$

The predicted failure compressive strengths of PSTC specimens obtained from the proposed empirical equation are given in Table 4. It is shown that, on average, the ratio of the predicted to the experimental results is equal to 1 with a COV of 4.3%, which confirms the accuracy of the proposed equation.

3.3 Ultimate strain

The axial strain of STCC columns is defined as the relative shortening of the concrete core in the longitudinal direction, while the lateral strain is the relative deformation of steel tube in the lateral direction. Since the steel tubes used in this study are thin-walled, the lateral strain of the steel tube was assumed to be equal to that of the concrete core. The ultimate axial and lateral strains of PSTC and NPSTC specimens under axial compression loads are presented in Table 5. It is shown that the ultimate strains of LPSTC specimens are very close to those of SPSTC

specimens. This indicates that increasing the prestressing level has a negligible effect on the ultimate axial and lateral strains of PSTC specimens. Also according to this table, the ultimate axial and lateral strains of NPSTC specimens are considerably higher (on average 20%) than those of PSTC specimens. The reason is that the initial circumferential strain of the steel tube in PSTC specimens (due to prestressing) reduces their strain and deformation capacity at the failure point. Also the concrete core in PSTC specimens is compressed, and therefore, its stiffness is much higher than that of the uncompressed concrete in NPSTC specimens, leading to lower deformations in PSTC specimens.

To predict the ultimate axial strain capacity of PSTC and NPSTC specimens, the relationship between the relative increase in the ultimate strain and the relative increase in the failure confined strength (compared with those of unconfined concrete) is investigated. The relative increase in the ultimate axial strain of PSTC and NPSTC specimens can be obtained, respectively, by using the nonlinear regression analysis of the results as Eqs. (19) and (20)

$$\left(\frac{\varepsilon_{af} - \varepsilon_{co}}{\varepsilon_{co}}\right) = 173.4 \left(\frac{f_{af} - f_{co}}{f_{co}}\right)^{0.379} \quad (19)$$

$$\left(\frac{\varepsilon_{pf} - \varepsilon_c}{\varepsilon_c}\right) = 162.4 \left(\frac{f_{pf} - f_c}{f_c}\right)^{0.272} \quad (20)$$

where ε_{af} and ε_{pf} are the ultimate axial strain of PSTC and NPSTC specimens, and ε_{co} and ε_c are the strain corresponding to the peak stress of the unconfined compressed and uncompressed concrete, respectively. The values of ε_{co} and ε_c for PSTC and NPSTC specimens are given in Table 5. Fig. 9 illustrates the relative increase in the ultimate axial strain versus the relative increase in the failure confined strength of PSTC and NPSTC specimens. The figure shows that the relative increase in the ultimate axial strain has a very good correlation with the relative increase in the failure confined strength.

According to the experimental results of this study, the ultimate lateral strain in PSTC and NPSTC specimens is always higher (on average 17%) than the corresponding

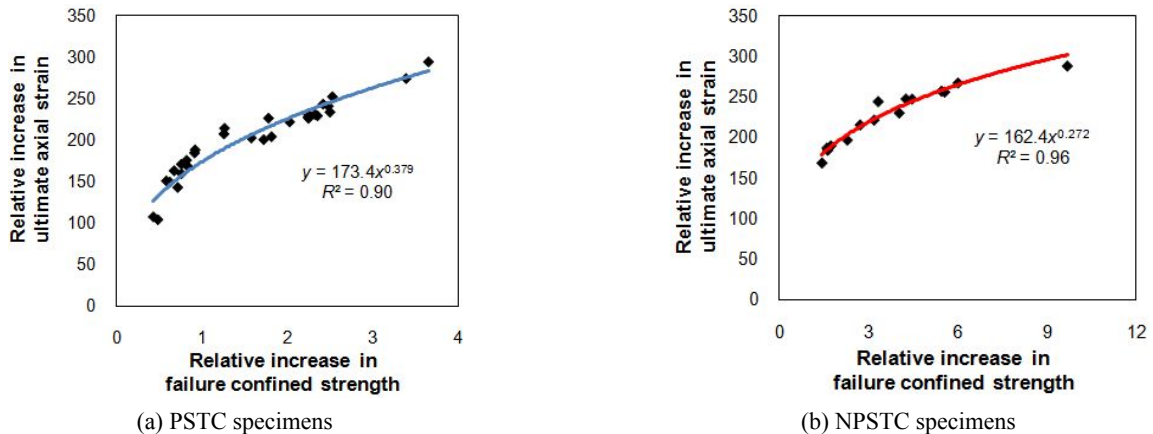| (a) PSTC specimens	(b) NPSTC specimens

Fig. 9 Relative increase in the ultimate axial strain versus relative increase in the confined strength

Table 5 Ultimate axial and lateral strains of the specimens

Specimen ID	Ultimate axial strain capacity	Ultimate lateral strain capacity	Axial strain at peak stress for unconfined concrete
L25P350-2.5	0.46	0.50	0.00199
S25P350-2.5	0.45	0.49	0.00196
N25P350-2.5	0.52	0.56	0.00202
L25P950-1.5	0.33	0.41	0.00206
S25P950-1.5	0.34	0.43	0.00202
N25P950-1.5	0.41	0.51	0.00207
L25P650-1.5	0.37	0.46	0.00200
S25P650-1.5	0.37	0.45	0.00196
N25P650-1.5	0.45	0.55	0.00202
L35P650-1.5	0.33	0.40	0.00218
S35P650-1.5	0.37	0.44	0.00210
N35P650-1.5	0.37	0.47	0.00218
L15P650-1.5	0.37	0.45	0.00178
S15P650-1.5	0.38	0.47	0.00177
N15P650-1.5	0.44	0.54	0.00190
L25P950-2.5	0.46	0.51	0.00203
S25P950-2.5	0.48	0.53	0.00199
N25P950-2.5	0.53	0.59	0.00205
L50P650-2.5	0.45	0.49	0.00220
S50P650-2.5	0.48	0.52	0.00207
N50P650-2.5	0.49	0.56	0.00226
L15P550-2.5	0.45	0.50	0.00164
S15P550-2.5	0.48	0.52	0.00163
N15P550-2.5	0.53	0.57	0.00183
L35P550-2.5	0.43	0.48	0.00214
S35P550-2.5	0.46	0.51	0.00207
N35P550-2.5	0.53	0.59	0.00213
L25P500-2.5	0.48	0.53	0.00197
S25P500-2.5	0.49	0.55	0.00194
N25P500-2.5	0.54	0.59	0.00201
L25P650-2.0	0.40	0.48	0.00197
S25P650-2.0	0.44	0.51	0.00194
N25P650-2.0	0.50	0.59	0.00201
L45P650-1.5	0.36	0.41	0.00220
S45P650-1.5	0.36	0.45	0.00210
N45P650-1.5	0.41	0.52	0.00221
L25P2000-1.0	0.21	0.26	0.00194
S25P2000-1.0	0.20	0.29	0.00191
N25P2000-1.0	0.38	0.50	0.00199
L47P650-1.5	0.33	0.39	0.00220
S47P650-1.5	0.30	0.34	0.00209
N47P650-1.5	0.42	0.52	0.00223
L55P650-2.5	0.50	0.50	0.00219
S55P650-2.5	0.48	0.49	0.00205
N55P650-2.5	0.56	0.60	0.00228

ultimate axial strain. This indicates that the ratio of the lateral strain to the axial strain (= Poisson's ratio) in PSTC and NPSTC specimens is larger than 1 at the failure point. This ratio is in the range of 1-1.45 and 1.07-1.32 for
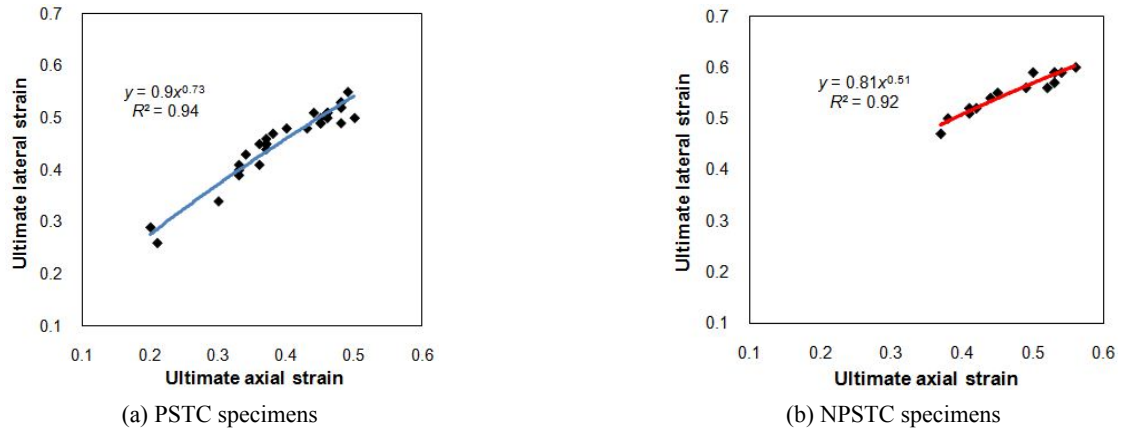
(a) PSTC specimens   (b) NPSTC specimens

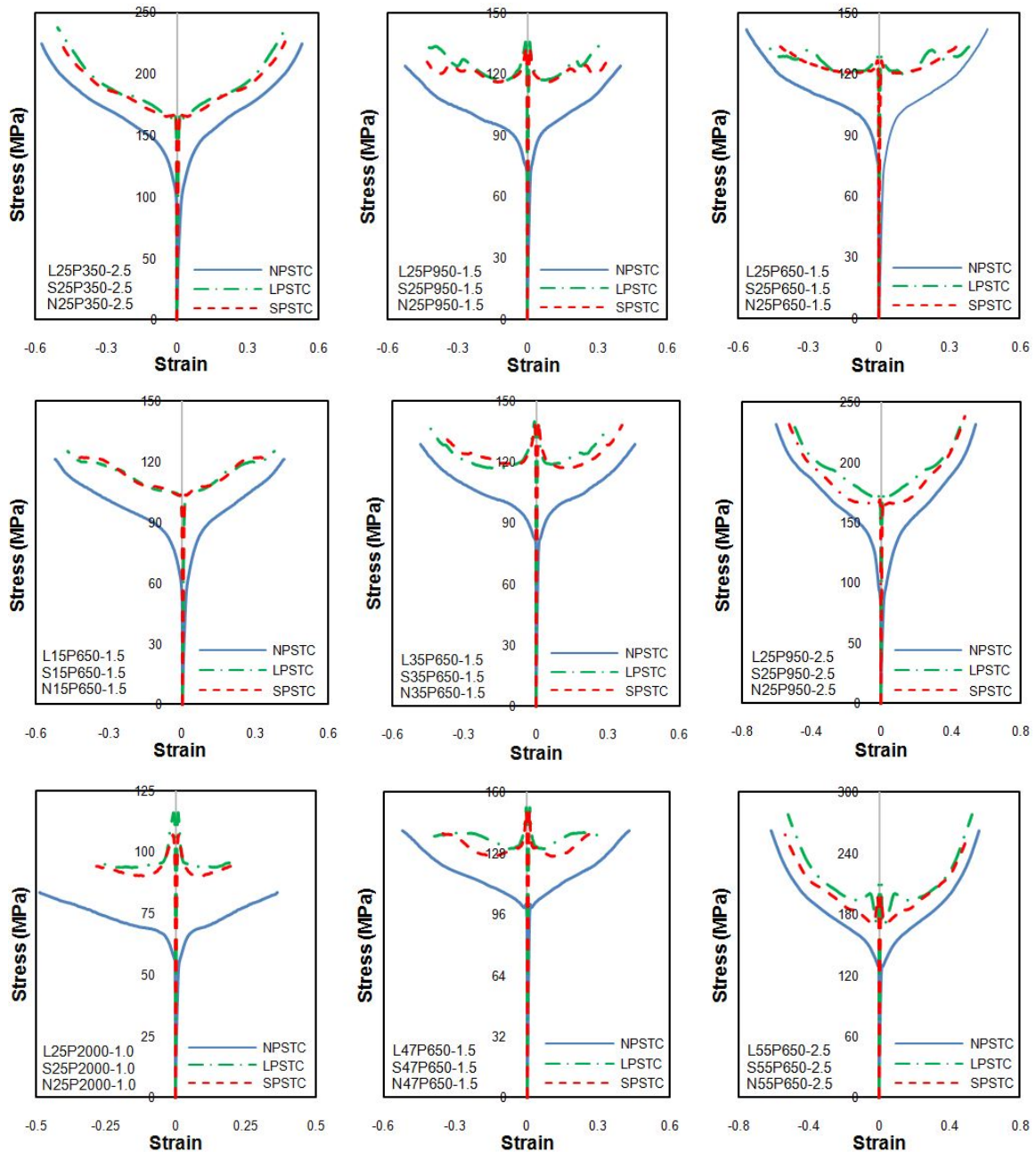Fig. 10 Ultimate lateral strain versus ultimate axial strain

Fig. 11 Axial and lateral stress–strain curves for LPSTC, SPSTC and NPSTC specimens

NPSTC and PSTC specimens, respectively. With increasing thickness of the steel tube, this ratio is reduced. The relationship between the ultimate axial strain and the ultimate lateral strain for PSTC and NPSTC specimens are shown in Fig. 10. Using nonlinear regression analysis, the following power functions are proposed for prediction of the ultimate lateral strain of PSTC and NPSTC specimens as a function of ultimate axial strain

$$\varepsilon_{afl} = 0.9\varepsilon_{af}^{0.73} \qquad \text{for PSTC specimens} \qquad (21)$$

$$\varepsilon_{pfl} = 0.81\varepsilon_{pf}^{0.51} \qquad \text{for NPSTC specimens} \qquad (22)$$

where ε_{afl} and ε_{pfl} are the ultimate lateral strain of PSTC and NPSTC specimens, respectively. It is shown in Fig. 10 that the proposed empirical equations can provide very accurate results for both PSTC and NPSTC specimens.

3.4 Stress-strain curve

Fig. 11 shows the axial and lateral stress-strain curves for NPSTC, SPSTC and LPSTC specimens under axial compression loads. As can be seen, the stress-strain curves for SPSTC and LPSTC are considerably higher than that of NPSTC specimens. This indicates that by applying pressure on the fresh concrete to create prestressing confinement loads, the mechanical properties of STCC columns are considerably improved. However, the lower ultimate strain of SPSTC and LPSTC specimens compared to that of NPSTC may lead to a lower failure compressive strength.

It can be found from Fig. 11 that the LPSTC stress–strain curve is almost coincident with that of SPSTC. Similar to the previous results, this observation shows that increasing the prestressing level has a negligible effect on improving the mechanical properties of PSTC specimens.

3.5 Failure mode

The failure of all STCC specimens was due to the rupture of the steel tube at the mid-height, as shown in Fig. 12. This is mainly because of the higher lateral deformation and the resulting stress at the mid-height of the steel tubes

Fig. 12 Failure mode of STCC specimen (left) and concrete core separated from the steel tube after failure point (right)

in comparison with the two ends of the specimens, due to the restraints at the ends. Since the failure was caused by the maximum shear stress at the mid-height of the steel tube, the ruptures occurred at almost 45 degrees to the horizontal. Similar behaviour can also be expected in the radial direction of the steel tube. This is confirmed by the oblique rupture in the wall thickness of the steel tube as shown in Fig. 12.

To investigate the condition of the concrete core at the failure point, the steel tube was removed from the concrete core of a confined concrete specimen (L50P650-2.5) that was loaded up to the failure, by cutting action (see Fig. 12). It can be concluded from the large deformations of concrete core that there was a significant displacement of aggregates into the hardened cement paste. To evaluate the load-carrying capacity of the concrete core after the failure point of STCC specimens, the concrete specimen was loaded under axial compression. The results showed that the concrete core still can withstand significant compressive loads (around 47.6 kN equivalent to 19.7 MPa), indicating that the concrete core did not reach its ultimate strength at the failure point.

4. Conclusions

This paper investigated the compressive behaviour of steel tube-confined concrete (STCC) stub columns with active and passive confinement. A total of 135 actively and passively confined specimens with different concrete compressive strength, outer diameter to wall thickness ratio of the steel tube and prestressing level were tested. The experimental results were then used to develop empirical equations to estimate the axial strength and the ultimate strain capacity of STCC stub columns with active and passive confinement. Based on the results of this study, the following conclusions can be drawn:

(1) Applying active confinement on STCC specimens leads to a considerable improvement in the axial and lateral stress-strain curves. It was shown that there is a negligible difference between the failure strength and stress-strain behaviour of SPSTC and LPSTC specimens. This indicates that using higher prestressing levels and keeping the applied pressure for a long time does not considerably affect the mechanical properties of actively confined specimens.

(2) With increasing the failure confinement ratio in actively and passively confined specimens, the relative increase in the failure confined strength increases. The confining pressure of PSTC specimens at the failure point is considerably higher than that of NPSTC specimens. The main reason is that the longitudinal to hoop stress ratio of steel tube in NPSTC specimens is almost two times higher than that of PSTC specimens at the failure point.

(3) By increasing the thickness of the steel tube, the failure compressive strength of PSTC and NPSTC specimens increases with a similar trend. The ultimate axial and lateral strains of NPSTC

specimens are on average 20% higher than that of PSTC specimens. The failure mode in both actively and passively confined specimens was due to the rupture of steel tube at the mid-height.

(4) The confinement effectiveness coefficient in passively confined specimens was 4.7, while in actively confined specimens it was between 1.7 and 4.1. This implies that the confinement effectiveness coefficient in actively confined specimens was 10% to 60% less than passively confined specimens.

(5) The proposed equations for prediction of the failure load-carrying capacity of passively and actively confined specimens (NPSTC and PSTC) show a very good agreement with the experimental results and, therefore, should prove useful in practical design of STCC columns with active and passive confinement.

References

ACI Committee 211.1-91 (2008), Standard practice for selecting proportions for normal, heavyweight, and mass concrete; ACI manual of concrete practice, Part 1, American Concrete Institute MI, USA, **38**.

Andrawes, B., Shin, M. and Wierschem, N. (2010), "Active confinement of reinforced concrete bridge columns using shape memory alloys", *J. Bridge Eng.*, **15**(1), 81-89.

ASTM A370 (2003), Standard test methods and definitions for mechanical testing of steel products; Annual Book of ASTM Standard 01.

Binici, B. (2005), "An analytical model for stress–strain behavior of confined concrete", *Eng. Struct.*, **27**(7), 1040-1051.

Chang, X., Huang, C.K. and Chen, Y.J. (2009), "Mechanical performance of eccentrically loaded pre-stressing concrete filled circular steel tube columns by means of expansive cement", *Eng. Struct.*, **31**(11), 2588-2597.

Dong, C.X., Kwan, A.K.H. and Ho, J.C.M. (2015), "A constitutive model for predicting the lateral strain of confined concrete", *Eng. Struct.*, **91**, 155-166.

Fam, A., Qie, F. and Rizkalla, S. (2004), "Concrete-filled steel tubes subjected to axial compression and lateral cyclic loads", *J. Struct. Eng.*, **4**(130), 631-640.

Fu, Z., Ji, B., Lv, L. and Yang, M. (2011), "The mechanical properties of lightweight aggregate concrete confined by steel tube", *Geotech. Sp. Publication ASCE*, **219**, 33-39.

Han, L.H., Yao, G.H., Chen, Z.B. and Yu, Q. (2005), "Experimental behaviour of steel tube confined concrete (STCC) columns", *Steel Compos. Struct., Int. J.*, **5**(6), 459-484.

Han, L.H., Liu, W. and Yang, Y.F. (2008), "Behavior of thin walled steel tube confined concrete stub columns subjected to axial local compression", *Thin-Wall. Struct.*, **46**(2), 155-164.

Helal, Y., Garcia, R., Pilakoutas, K., Guadagnini, M. and Hajirasouliha, I. (2016), "Strengthening of short splices in RC beams using Post-Tensioned Metal Straps", *Mater. Struct.*, **49**(1-2), 133-147.

Hosford, W. (2010), *Solid Mechanics*, University of Michigan, Emeritus, Cambridge University Press, 262 p.

Huang, Y., Xiao, J. and Zhang, C. (2012), "Theoretical study on mechanical behavior of steel confined recycled aggregate concrete", *J. Constr. Steel Res.*, **76**, 100-111.

Janke, L., Czaderski, C., Ruth, J. and Motavalli, M. (2009), "Experiments on the residual load-bearing capacity of prestressed confined concrete columns", *Eng. Struct.*, **31**(10), 2247-2256.

Krstulovic-Opara, N. and Thiedeman, P.D. (2000), "Active confinement of concrete members with self-stressing composites", *ACI Mater. J.*, **97**(3), 297-308.

Lahlou, K., Lachemi, M. and Aitcin, P.C. (1999), "Behavior of HSC filled tube columns under dynamic compressive loading", *ASCE J. Struct. Eng.*, **125**(10), 1100-1108.

Mander, B.J., Priestley, J.N.M. and Park, R. (1988), "Theoretical stress–strain model for confined concrete", *ASCE J. Struct. Eng.* **144**(8), 1804-1826.

Moghaddam, H., Samadi, M., Pilakoutas, K. and Mohebbi, S. (2010), "Axial compressive behavior of concrete actively confined by metal strips; Part A: Experimental study", *Mater. Struct.*, **43**(10), 1369-1381.

Mortazavi, A.A., Pilakoutas, K. and Son, K.S. (2003), "RC column strengthening by lateral pre-tensioning of FRP", *J. Constr. Build. Mater.*, **6-7**(17), 363-518.

Nemati, S.T. (2006), *Effect of Active Confinement on Concrete Behavior*, Dissertation for Master's Degree; Mazandaran University, Iran.

Nematzadeh, M. (2012), *Determining the Relationships of Active Confinement of Fresh Concrete by Prestressing Steel Tubes*, Dissertation for Doctoral Degree; Mazandaran University, Iran.

Nematzadeh, M. and Naghipour, M. (2012), "Compressive strength and modulus of elasticity of freshly compressed concrete", *Constr. Build. Mater.*, **34**, 476-485.

Nematzadeh, M., Fazli, S. and Hajirasouliha, I. (2017), "Experimental study and calculation of laterally-prestressed confined concrete columns", *Steel Compos. Struct., Int. J.*, **23**(5), 517-527.

O'Shea, M.D. and Bridge, R.Q. (1998), "Tests on circular thin-walled steel tubes filled with medium and high strength concrete", *Australian Civil Eng. Trans.*, **40**, 15-27.

Qi, H., Guo, L., Liu, J., Gan, D. and Zhang, S. (2011), "Axial load behavior and strength of tubed steel reinforced-concrete (SRC) stub columns", *Thin-Wall. Struct.*, **49**(9), 1141-1150.

Richart, F.E., Brandtzaeg, A. and Brown, R.L. (1928), "A study of the failure of concrete under combined compressive stresses", Bulletin 185; University of Illinois Engineering Experimental Station, Champaign, IL, USA.

Shin, M. and Andrawes, B. (2014), "Parametric study of RC bridge columns actively confined with shape memory alloy spirals under lateral cyclic loading", *J. Bridge Eng.*, **19**(10).

Shinohara, Y. (2008), "Effect of transverse prestressing on shear behaviors of high-strength concrete columns", *Proceedings of the 14th World Conference on Earthquake Engineering* (14WCEE), Beijing, China, October.

Vincent, T. and Ozbakkaloglu, T. (2015), "Compressive behavior of prestressed high-strength concrete-filled aramid FRP tube columns: Experimental observations", *J. Compos. Constr.*, **19**(6), 1-13.

Xiao, Y., He, W.H. and Choi, K.K. (2005), "Confined concrete-filled tubular columns", *J. Struct. Eng. ASCE*, **131**(3), 488-497.

Yu, Q., Tao, Z., Liu, W. and Chen, Z.B. (2010), "Analysis and calculations of steel tube confined concrete (STCC) stub columns", *J. Constr. Steel Res.*, **66**(1), 53-64.

DL

Nomenclature

STCC	:	Steel Tube-Confined Concrete
LPSTC	:	Long-term Prestressed Steel Tube-Confined Compressed Concrete
SPSTC	:	Short-term Prestressed Steel Tube-Confined Compressed Concrete
NPSTC	:	Non-Prestressed Steel tube-Confined Concrete
PSTC	:	Prestressed Steel tube-Confined Compressed Concrete
COV	:	Coefficient of variation

Notation

A_c	Cross-sectional area of concrete		P_i	Initial lateral pressure
A_s	Cross-sectional area of steel tube		P_r	Prestressing ratio
C_r	Confinement ratio		P_{af}	Load-carrying capacity of PSTC
C_{ru}	Confinement ratio at failure point		t	Steel tube wall thickness
D	External diameter of steel tube		α	Longitudinal to hoop stress ratio of steel tube at failure point
E_s	Initial modulus of elasticity of steel		ε_c	Axial strain of unconfined concrete at the maximum stress
E'_s	Strain hardening modulus of elasticity of steel		ε_y	Axial strain of steel tube at yielding point
f_c	Compressive strength of unconfined concrete		ε_u	Steel ultimate strain
f_l	Lateral confining pressure		ε_{af}	Ultimate axial strain of PSTC
f_y	Steel yield strength		ε_{afl}	Ultimate lateral strain of PSTC
f_{af}	Confined compressive strength of PSTC at failure point		ε_{co}	Axial strain of compressed concrete at the maximum stress
f_{cc}	Compressive strength of confined concrete		ε_{pf}	Ultimate axial strain of NPSTC
f_{co}	Compressive strength of unconfined compressed concrete		ε_{pfl}	Ultimate lateral strain of NPSTC
f_{lu}	Lateral confining pressure at failure point		ε_p	Axial strain of steel tube at strain hardening point
f_{pf}	Confined compressive strength of NPSTC at failure point		v_s	Poisson's ratio of steel tube
f_{us}	Steel ultimate strength		σ_z	Longitudinal stress of steel tube
K	Confinement effectiveness coefficient		σ_θ	Hoop stress of steel tube
P_f	Final lateral pressure (Prestressing level)			